BIOCHEMISTRY
including biophysical chemistry & molecular biology

Article

pubs.acs.org/biochemistry

Chemical Mechanism of Glycerol 3-Phosphate Phosphatase: pH-Dependent Changes in the Rate-Limiting Step

Gérald Larrouy-Maumus,[†] Geoff Kelly,[‡] and Luiz Pedro Sório de Carvalho*[,†]

[†]Mycobacterial Research Division, MRC, National Institute for Medical Research, and [‡]MRC Biomolecular NMR Centre, The Ridgeway, Mill Hill, London NW7 1AA, U.K.

Supporting Information

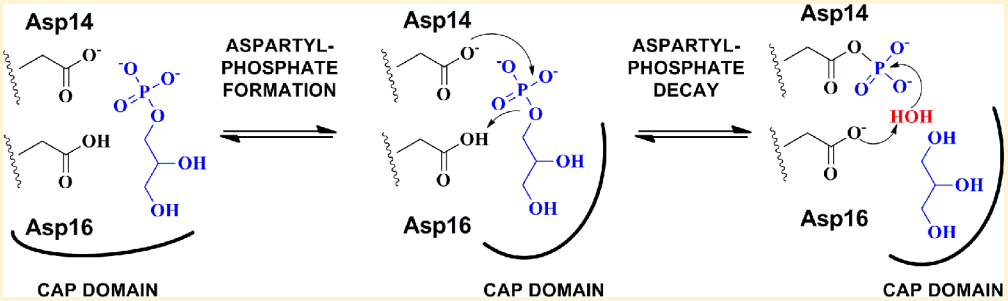

ABSTRACT: The halo-acid dehalogenase (HAD) superfamily comprises a large number of enzymes that share a conserved core domain responsible for a diverse array of chemical transformations (e.g., phosphonatase, dehalogenase, phosphohexomutase, and phosphatase) and a cap domain that controls substrate specificity. Phosphate hydrolysis is thought to proceed via an aspartyl-phosphate intermediate, and X-ray crystallography has shown that protein active site conformational changes are required for catalytic competency. Using a combination of steady-state and pre-steady-state kinetics, pL−rate studies, solvent kinetic isotope effects, ^{18}O molecular isotope exchange, and partition experiments, we provide a detailed description of the chemical mechanism of a glycerol 3-phosphate phosphatase. This phosphatase has been recently recognized as a rate-limiting factor in lipid polar head recycling in *Mycobacterium tuberculosis* [Larrouy-Maumus, G., et al. (2013) *Proc. Natl. Acad. Sci. 110* (28), 11320−11325]. Our results clearly establish the existence of an aspartyl-phosphate intermediate in this newly discovered member of the HAD superfamily. No ionizable groups are rate-limiting from pH 5.5 to 9.5, consistent with the p*K* values of the catalytic aspartate residues. The formation and decay of this intermediate are partially rate-limiting below pH 7.0, and a conformational change preceding catalysis is rate-limiting above pH 7.0.

Enzymes from the halo-acid dehalogenase superfamily (HADSF) are ubiquitous in nature, with multiple members typically present in a single organism (e.g., 183 in humans, 37 in *Escherichia coli*, and 30 in *Mycobacterium tuberculosis*). They are responsible for a wide range of vital biological functions, such as primary metabolism,[1] transport,[2] signal transduction,[3,4] transcription,[5] and DNA repair.[6] Members of the HADSF catalyze group transfer reactions mediated by an active site aspartate nucleophile.[7] Members of the HADSF with known function fall into one of five functional classes: haloalkanoate dehalogenases (C−C bond hydrolysis), phosphonoacetaldehyde hydrolases (P−C bond hydrolysis), phosphonate monoesterases (P−O−C bond hydrolysis), ATPases (P−O−P bond hydrolysis), and phosphomutases (P−O−C bond cleavage, with intramolecular phosphoryl transfer).[8] Members of the HADSF contain a conserved mixed α/β Rossmann fold and a catalytically essential nucleophilic aspartate residue.[7] On the basis of additional structural elements that are inserted into the Rossmann fold, HADSF enzymes are divided into three subfamilies.[9] Members of subfamilies I and II are usually monomeric and contain a structural insertion termed the cap domain.[8−10] The cap domain acts as a "lid" to cover the substrate in the active site, thereby ensuring catalytic efficiency.[8] In contrast, members of subfamily III lack the cap domain and generally exhibit broad substrate specificity.[8,11]

A great deal of effort has been focused on understanding substrate specificity and associated structural determinants of phosphohydrolases/transferases belonging to the HADSF.[8−10] However, in contrast to those of small tyrosine phosphatases,[12−17] alkaline phosphatases,[18−22] and prostatic phosphatase,[23] the detailed chemical mechanism of enzymes belonging to the HADSF remains poorly understood.

The HADSF phosphotransferases share a core domain that binds a divalent cation, usually Mg^{2+}, and the organophosphate substrate in an orientation that allows attack by the conserved Asp nucleophile and general acid/base catalysis by a second Asp positioned two residues upstream (Asp+2 residue).[1,9] The proposed general catalytic mechanism, shown in Scheme 1A, consists of two parts: (1) nucleophilic attack by the first

Received: July 2, 2013
Revised: December 12, 2013
Published: December 20, 2013

   dx.doi.org/10.1021/bi400856y | *Biochemistry* 2014, 53, 143−151

Scheme 1. Proposed Mechanisms for Hydrolysis of Glycerol 3-Phosphate Catalyzed by MtGPP

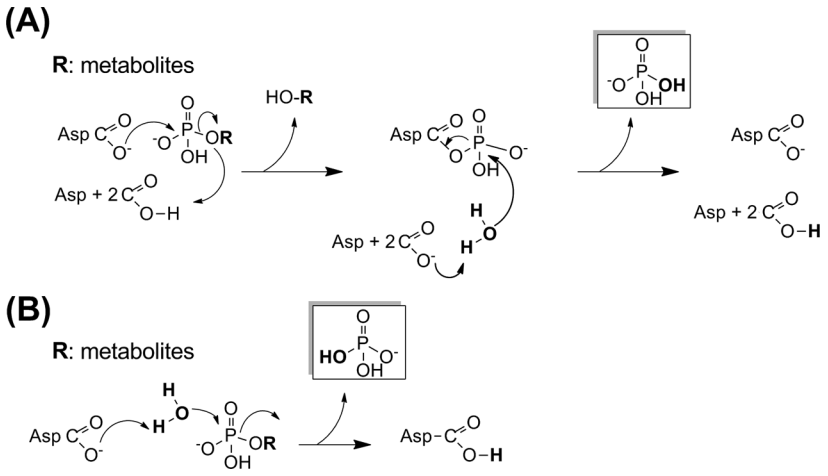

conserved Asp residue resulting in formation of the first product and an aspartyl-phosphate intermediate and (2) activation of a water molecule by the second conserved Asp residue and its attack on the phosphorylated Asp residue leading to the breakdown of the phosphoenzyme intermediate and release of inorganic phosphate, the second product (Scheme 1A). An alternative mechanism would involve activation of a water molecule (perhaps by one of the conserved aspartate residues), and subsequent direct attack of the phosphorylated substrate, leading to the release of inorganic phosphate and the dephosphorylated product, without the formation of a phosphoenzyme intermediate (Scheme 1B). As crystallographic evidence of an aspartyl-phosphate intermediate is lacking in most published cases, mechanistic studies can provide definitive proof of the mechanism in question.

Recently, we have identified a novel glycerol 3-phosphate phosphatase (MtGPP), encoded by the *rv1692* gene.[24] MtGPP is involved in phospholipid polar head recycling/catabolism in *M. tuberculosis*. According to the primary sequence and crystal structure, MtGPP is composed of a conserved catalytic core domain and a cap domain. MtGPP belongs to HAD subfamily IIA, characterized by the location of the cap domain between motifs II and III of the core domain and the presence of two different α/β folds, designated types IIA and IIB. In contrast to most of the other members of the HADSF, a GCN5-related *N*-acetyltransferase (GNAT)-like domain was identified at the C-terminal region of the protein. This fused GNAT region appears to be required only for protein stability and/or solubility.

Here we report a detailed mechanistic characterization of MtGPP catalysis using pH−rate studies, solvent kinetic isotope effects, molecular isotope exchange, ^{1}H, ^{13}C, and ^{31}P nuclear magnetic resonance (NMR), transient kinetics, and partition experiments. Chemistry proceeds via the formation of an aspartyl-phosphate intermediate, and its breakdown is partially rate-limiting and reversible.

MATERIALS AND METHODS

Materials. Buffers and sodium chloride were purchased from Fisher Scientific. Unless otherwise stated, all other chemicals were purchased from Sigma-Aldrich. Chromatographic columns were purchased from GE Healthcare, and Ni-NTA resin was from EMD. Complete EDTA-free protease inhibitor was purchased from Roche. BL21(DE3)pLysS was from EMD.

General Methods and Equipment. The protein concentration was measured using the bicinchoninic acid (BCA) assay (Thermo Scientific), using bovine serum albumin as the standard. Protein purification was performed using an ÅKTA purifier 10 (GE). Sodium dodecyl sulfate−polyacrylamide gel electrophoresis (SDS−PAGE) was performed on a PhastSystem (GE). Spectrophotometry was conducted with a Shimadzu UV-2550 spectrophotometer equipped with dual-beam optics and a Peltier system for temperature control. Stopped-flow absorbance spectroscopy was conducted on an Applied Photophysics SX-20 stopped-flow spectrophotometer (10 mm path length), equipped with a circulating water bath. Under the conditions employed, the dead time was estimated to be 3 ms. Experiments were initiated by mixing equal volumes of two solutions, one containing substrate and the other enzyme. ^{1}H and ^{31}P NMR spectroscopy were conducted on a Varian Inova 600 MHz NMR spectrometer. All assays were conducted at 25 °C. All concentrations of MtGPP reported are final concentrations employed, for the monomeric form of the enzyme.

Preparation of Recombinant MtGPP. Recombinant MtGPP was expressed and purified to homogeneity as described previously.[24] Briefly, *rv1692* was amplified from Mtb H37Rv genomic DNA using primers gccatatggcacaccaccaccaccaccatgaaaagcattgcgcagg and gcaagctttcattgcgttcctacgctag and cloned into the *Nde*I and *Hin*dIII sites of pET23a(+). Protein expression was conducted in BL21(DE3) pLysS cells cultured in LB broth, at 37 °C. All purification steps were conducted at 4 °C. The cell pellet was resuspended in 20 mM triethanolamine (TEA) (pH 7.8) containing two tablets of complete protease inhibitor cocktail, and 50 μL of TurboDNase (Ambion) (2 units/μL). The cells were disrupted by sonication and clarified by centrifugation at 25000*g* for 30 min. The supernatant was applied to a 50 mL column of Ni-NTA His Bind Superflow resin equilibrated with buffer A [20 mM TEA (pH 7.8), 50 mM imidazole, and 300 mM NaCl]. The column was washed once with 220 mL of buffer A, and protein was eluted with a linear gradient of 50 to 500 mM imidazole in buffer A (570 mL). The fractions containing MtGPP were pooled and dialyzed thrice against 4 L of 20 mM TEA (pH 7.8). The enzyme was concentrated to 14 mg/mL, flash-frozen, and stored at −80 °C. Purified recombinant His-tagged MtGPP

dx.doi.org/10.1021/bi400856y | *Biochemistry* 2014, 53, 143−151

migrated as a single band by SDS−PAGE (Coomassie blue staining indicated >95% purity) and was stable at 4 °C for prolonged periods of time (hours to days). The total yield of recombinant MtGPP was 12.8 mg/g of pelleted cells. ESI-MS analysis of recombinant MtGPP recorded a molecular mass of 37903.6 Da (calculated molecular mass of 37903.8 Da).

Measurement of Enzymatic Activity (steady-state kinetics). All initial velocities for the forward reaction of MtGPP with glycerol 3-phosphate as the substrate were determined at 25 °C in 50 mM Tris-HCl and 2 mM $MgCl_2$ (pH 7.5) using a coupling assay (EnzCheck phosphate assay kit, Invitrogen) to permit spectrophotometric detection of product formation (as per the manufacturer's instructions). Alternatively, when *p*-nitrophenyl phosphate (*p*NPP) was used as a substrate, catalytic activity was followed by direct spectrophotometric detection of *p*-nitrophenolate formation (ε_{405} = 13435 M^{-1} cm^{-1}, at pH 7.5). Reactions were initiated by the addition of enzyme, typically to a final concentration of 40 nM.

Determination of the Extinction Coefficient of *p*-Nitrophenolate at Different pH Values. The extinction coefficient was determined at 25 °C by varying the concentration of *p*-nitrophenolate (0.02−4 mM) according to Lambert−Beer's law. The following buffers were used for the indicated pH ranges: 2-(*N*-morpholino)ethanesulfonic acid (MES) for pH 5.0, 5.5, 6.0, and 6.5; piperazine-*N*,*N*′-bis(2-ethanesulfonic acid) (PIPES) for pH 7.0; 4-2-hydroxyethyl-1-piperazineethanesulfonic acid (HEPES) for pH 7.5; *N*-tris(hydroxymethyl)methyl-2-aminopropanesulfonic acid (TAPS) for pH 8.0 and 8.5; and 2-(*N*-cyclohexylamino)ethanesulfonic acid (CHES) for pH 9.0 and 9.5.

pL Studies. The pL (L = H or D) dependence of V (k_{cat}) and V/K (k_{cat}/K_m) was determined at 25 °C using *p*NPP as the substrate (see above for buffers employed). Saturation curves were fit using eq 1. For the pD dependence, the values of the buffer solutions were adjusted according to the relationship pD = pH + 0.4.

Solvent Kinetic Isotope Effects. Solvent kinetic isotope effects (SKIEs) on k_{cat} and K_m were measured by obtaining saturation curves of MtGPP-catalyzed *p*NPP hydrolysis in either pure H_2O or pure D_2O (99.6% pure) and applying parameters to eq 2 (where F_i = 0 for H_2O and F_i = 0.996 for D_2O). SKIEs were measured between pL 5.5 and 9.5. A proton inventory on V_{max} was performed at pL 6.0 by varying the atom fraction of deuterium oxide from 0 to 0.8 in increments of 0.2 and measuring the MtGPP activity in the presence of saturating concentrations of *p*NPP. Each data point was determined in quadruplicate. The data were fit using eq 3.

Solvent Viscosity. The effect of viscosity on the reaction catalyzed by MtGPP was evaluated by following the reaction with *p*NPP in the absence or presence of 9% glycerol, at 25 °C in 50 mM Tris-HCl and 2 mM $MgCl_2$. Solvent viscosity was evaluated at pH 6.0 and 8.5. No effect of glycerol on the extinction coefficient was observed under these experimental conditions (Table S1 of the Supporting Information).

Pre-Steady-State Kinetics. All experiments were performed at 25 °C in 50 mM Tris-HCl and 2 mM $MgCl_2$ (pH 7.5). Replicate progress curves (generally 5−10 shots) were averaged and fit using eq 4. Multiple turnovers were measured by monitoring the increase in absorbance due to *p*-nitrophenolate formation (ε_{405} = 13435 M^{-1} cm^{-1}). The photomultiplier voltage corresponding to zero absorbance was set using *p*NPP in the observation cell. For these experiments, the final concentration of *p*NPP was saturating (40 mM), while the final MtGPP concentration was varied from 5 to 100 μM.

Molecular Isotope Exchange (MIX). All MIX reactions were performed with 2 μM MtGPP in 50 mM Tris-HCl and 2 mM $MgCl_2$ (pH 7.5) at 25 °C in 92% $H_2{}^{18}O$ and quenched by addition of 8 mM EDTA. The phosphatase activity of MtGPP was determined using 10 mM D,L-glycerol 3-phosphate. $H_2{}^{18}O-P_i$ exchange catalyzed by MtGPP was conducted by incubating 10 mM inorganic phosphate in the presence of enzyme at 92% $H_2{}^{18}O$. ^{31}P NMR was used to follow the exchange process based on the observation that the ^{18}O isotope caused an upfield shift in the ^{31}P NMR signal.[25] Spectra were recorded on a Varian Inova 600 MHz NMR spectrometer (128 scans, 242.5 MHz).

Partition Experiments. The effects of methanol (MeOH) on the initial rate of phosphatase activity, with *p*NPP as the substrate, were determined spectrophotometrically, as described above, in an aqueous MeOH/50 mM HEPES mixture and 2 mM $MgCl_2$ (pH 7.5). The MeOH concentration was varied from 0 to 6 M.

Data Analysis. Data were fit using the nonlinear least-squares curve-fitting programs of SigmaPlot version 11.0 (SysTat Software Inc.). Individual saturation curves were fit using eq 1:

$$v = (VS)/(S + K) \tag{1}$$

where v is the maximal velocity, S is the substrate concentration, and K is the Michaelis constant (K_m). Solvent kinetic isotope and viscosity effects were fit using eq 2:

$$v = (VS)/[K(1 + F_iE_{V/K}) + S(1 + F_iE_V)] \tag{2}$$

where F_i is the fraction of the isotopic label and E_V and $E_{V/K}$ are the isotope effects minus one on V and V/K, respectively. The linear proton inventory on V_{max} was fit using eq 3:

$$V_o/V_n = 1 - n + n(k_H/k_D) \tag{3}$$

where n is the atom fraction of deuterium in the mixed isotopic solvent, V_n is the velocity in the solvent at atom fraction of deuterium n, V_o is the velocity in pure H_2O, and k_D/k_H is the isotopic effect. Stopped-flow absorbance traces obtained under multiple-turnover conditions were fit using eq 4:

$$y(t) = \sum_i A_i e^{-k_i t} + vt + C \tag{4}$$

where $y(t)$ is the observed signal at time t, i is the number of transients, A_i is the amplitude of the ith transient, k_i is the observed rate constant (k_{obs}) for the ith transient, v is the steady-state velocity, and C is the offset.

RESULTS AND DISCUSSION

Purification of MtGPP. MtGPP was expressed in *E. coli* BL21(DE3)pLysS cells and purified to homogeneity using Ni-NTA chromatography, as described previously.[24]

pH Dependence of the Kinetic Parameters of MtGPP. The pH dependence of V is obtained at saturating concentrations of substrate, while V/K versus pH is obtained at limiting concentrations of substrate. The V versus pH profile will thus report on groups within the enzyme−substrate complex required for catalysis, while the V/K versus pH profile will report on ionizable groups of the free enzyme and/or reactant important for binding and/or catalysis.[26,27] For MtGPP, the pH dependences of V and V/K were examined

dx.doi.org/10.1021/bi400856y | *Biochemistry* 2014, 53, 143−151

Table 1. Comparison of Solvent Kinetic Isotope Effects and Solvent Viscosities for the Hydrolysis of *p*NPP by MtGPP

	D_2O		relative viscosity[a]	
pL	V/K[b]	V	V/K	V
6.0	1.83 ± 0.28[c] (2.01 ± 0.41)[d]	1.87 ± 0.08 (2.56 ± 0.15)[d]	0.91 ± 0.12	0.73 ± 0.03
7.5	0.76 ± 0.06	1.06 ± 0.02	nd[e]	nd[e]
8.5	0.64 ± 0.13 (0.89 ± 0.24)[d]	0.68 ± 0.04 (0.79 ± 0.06)[d]	0.72 ± 0.13	0.86 ± 0.05

[a]For these experiments, 9% glycerol was used as a viscogen to emulate the viscosity of 100% D_2O. [b]Kinetic parameters are reported as the ratio of values (H_2O/D_2O). [c]Values reported in the table are the averages of at least two independent experiments. [d]Values in parentheses are corrected for the viscosity with 9% glycerol. [e]Not determined.

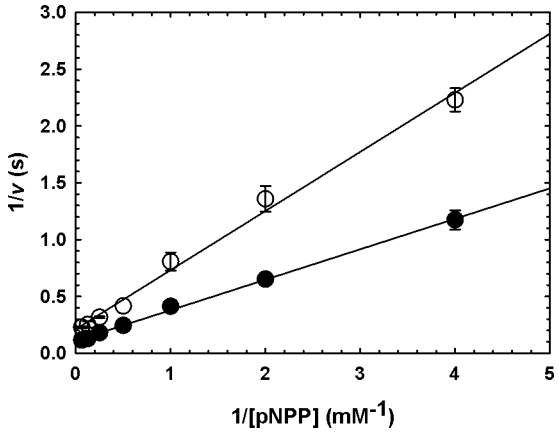

Figure 1. Solvent kinetic isotope effects at pL 6.0 in H_2O (●) and 99.6% D_2O (○). Data were fit to eq 2, which gave a ^{D}V of 1.83 ± 0.28 and a $^{D}V/K$ of 1.87 ± 0.08.

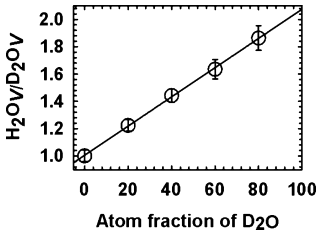

Figure 2. Proton inventory for V of the hydrolysis of *p*NPP by MtGPP at pL 6.0 at 25 °C. Symbols are data, and the line is the fit to eq 3.

between pH 5.5 and 9.5, using *p*NPP as the substrate (Figure S1 of the Supporting Information). Extinction coefficients were experimentally determined for *p*-nitrophenolate at each pH, as *p*-nitrophenolate's absorbance is strongly pH dependent (Table S1 of the Supporting Information). As one can see in Figure S1 of the Supporting Information, no ionizable groups could be defined in this range for either V or V/K. However, both V and V/K profiles display modest downward curvature at higher pH values. The lack of ionizable groups for either V or V/K in this pH range suggests that the pH-dependent step is not originally rate-limiting. In this case, both aspartate residues are likely in the correct protonation state in the range studied. Furthermore, substrate ionizations should not be visible in V profiles as glycerol phosphate and *p*NPP are expected to bind only in the properly ionized form (i.e., dianion).[28] As a control, the activity of MtGPP was assayed in the presence of increasing concentrations of NaCl. Inhibition was observed at millimolar concentrations of NaCl (Figure S5 of the Supporting Information), which are likely not causing the effects observed in the pH−rate studies.

Solvent Kinetic Isotope Effects (SKIEs). Solvent isotope effects were employed to study the chemical mechanism of MtGPP hydrolysis of *p*NPP (Table 1 and Figures S2−S4 of the Supporting Information). The pH dependence of both ^{D_2O}V and $^{D_2O}V/K$ is complex, displaying both normal and inverse isotope effects. $^{D_2O}V/K$ is highest at low pH (5.5), and its magnitude decreases as the pH is increased, reaching unity at pH 7.0 and becoming slightly inverse until the pH reaches 9.5 (Table 1 and Figure S3 of the Supporting Information). In contrast, ^{D_2O}V is unity at pH 5.5, increases to ∼2.4 at pH 6.8, then decreases again, and becomes inverse until the pH reaches 9.5 (Table 1 and Figure S4 of the Supporting Information). These results indicate that chemistry is rate-limiting for MtGPP at pH ≤7.0 under V/K conditions and at pH 7.0 under V conditions. In addition, this reverse behavior observed with SKIEs indicates that V/K and V are likely reporting on distinct segments of the catalytic mechanism. Assuming the first irreversible step is the formation of the aspartyl-phosphate intermediate and release of glycerol, it is tempting to propose that formation of this intermediate is represented by $^{D_2O}V/K$ and its hydrolysis by ^{D_2O}V.

The apparent inverse SKIEs found at neutral and basic pH values for both V and V/K have not previously been reported for phosphatases belonging to the HADSF. Inverse solvent isotope effects are commonly attributed to proton transfer processes involving groups that exhibit inverse fractionation factors. Known causes of inverse fractionation factors include the increased viscosity of D_2O,[29] metal-bound water molecules (∼0.7−1.0), a CysSH/$CysS^-$ + H^+ equilibrium (∼0.5), and conformational changes with fractionation factors of less than unity.[29−31] As there are no Cys residues near the catalytic site, deprotonation of CysSH is unlikely to cause the observed inverse effects. Conformational changes do occur when enzymes belonging to the HADSF bind their substrates, and divalent cation−product dissociation must occur during turnover,[32] making both potential origins of the inverse SKIE. In a few cases,[29,31] apparent inverse SKIEs were shown to arise from solvent viscosity, rather than from chemical steps.[29] Consequently, we performed viscosity experiments to probe this possibility, by comparing the rate of MtGPP turnover in the presence and absence of 9% glycerol as a viscogen, which emulates the viscosity of 100% D_2O. As shown in Table 1, increasing the solvent viscosity increases the rate of MtGPP activity, at both pL 6.0 and 8.5 (H_2O/viscogen ratios of V and V/K between 0.72 and 0.91). Eliminating this effect on the observed SKIEs yields the corrected data listed in Table 1. Upon correction, we can observe a normal solvent kinetic isotope effect for both V and V/K at pL 6.0. It is also apparent from these data that at pL 6.0 chemistry is partially rate-limiting (Figure 1), evidenced by indistinguishable normal SKIEs. In contrast, at pL 8.5, $^{D_2O}V/K$ and ^{D_2O}V are slightly inverse, 0.79 and 0.89, respectively. Altogether, viscosity-corrected SKIE results obtained with *p*NPP suggest that the chemical steps are rate-limiting in the reaction catalyzed by MtGPP.

Proton Inventory. The proton inventory method allows one to obtain information about the number of hydrogenic sites contributing to the overall solvent isotope effect and the magnitude of the individual isotope effects or fractionation factors. In our experiments, $^{H_2O}V/^{D_2O}V$ was determined in 20%

dx.doi.org/10.1021/bi400856y | *Biochemistry* 2014, 53, 143−151

Scheme 2. ^{18}O MIX Experiments Conducted with MtGPP

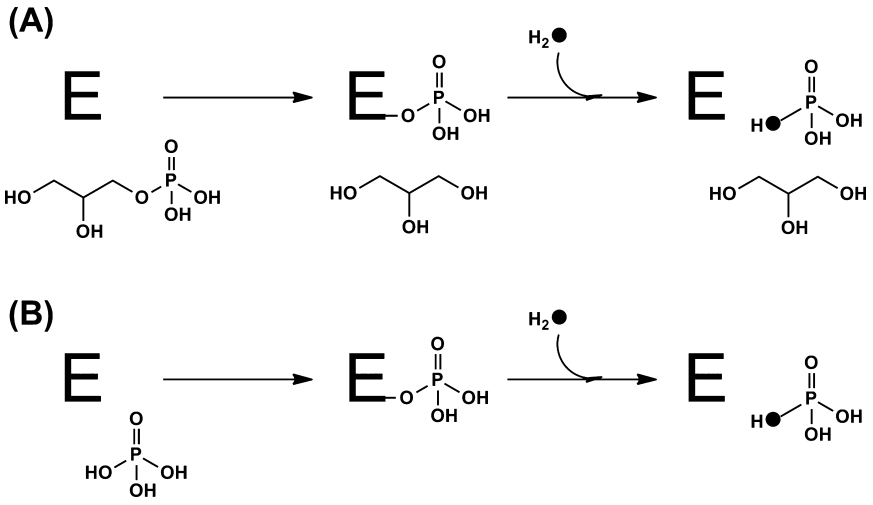

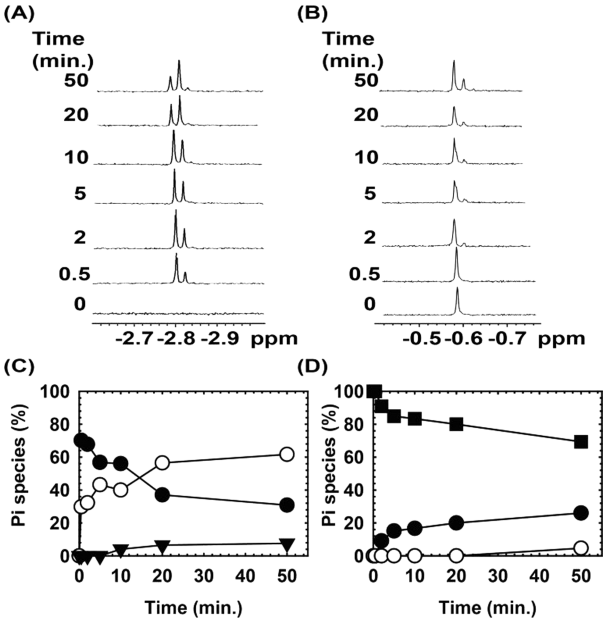

Figure 3. Isotope exchange experiment with the ^{18}O probe conducted by one-dimensional ^{31}P NMR. (A) Time course of the hydrolysis of glycerol 3-phosphate hydrolysis by MtGPP. (B) Time course of the inorganic phosphate oxygen exchange catalyzed by MtGPP, in the absence of glycerol 3-phosphate. (C and D) Plots showing the percentage of P_i species from the hydrolysis of glycerol 3-phosphate and inorganic phosphate oxygen exchange, respectively: (■) $[P^{16}O_4]$, (●) $[P^{18}O^{16}O_3]$, (○) $[P^{18}O_2{}^{16}O_2]$, and (▼) $[P^{18}O_3{}^{16}O_1]$.

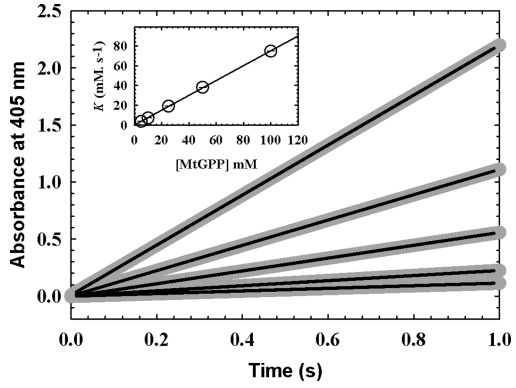

Figure 4. Multiple-turnover experiments with MtGPP. Representative reaction traces under multiple-turnover conditions obtained at different concentrations of MtGPP and fixed saturating concentrations of *p*NPP (40 mM). The solid gray line is data, an average of 10 traces, and the solid black line is the fit to eq 4. The inset shows the plot of k_{obs} vs MtGPP concentration. Symbols represent data, and the solid line is a best fit to a linear polynomial equation. Reactions were conducted in 50 mM Tris-HCl and 2 mM $MgCl_2$ (pH 7.5), with 40 mM *p*NPP and 5−100 μM MtGPP, at 25 °C. Results are representative of two independent experiments.

Scheme 3. Partition Experiment

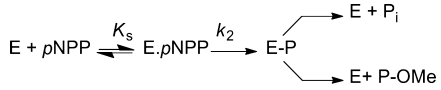

increments from 0 to 80% D_2O, at pL 6.0, where chemistry is largely rate-limiting and likely reporting on aspartyl-phosphate hydrolysis (Figure 2). A linear proton inventory (slope of 1.011 ± 0.001) was obtained for the hydrolysis of *p*NPP by MtGPP. This suggests that a single solvent-exchangeable proton is in flight in the transition state for hydrolysis of the aspartyl-phosphate intermediate (probed under *V* conditions). The simplest model that accounts for this effect with the structural evidence currently available is that Asp+2 deprotonates a water molecule, which in turns attacks the phosphate, with Asp as the leaving group.

Formation and Decomposition of the Phosphoenzyme Intermediate. Isotope (^{18}O)-induced shifts in ^{31}P NMR resonances have previously been applied to study enzyme-catalyzed phosphate exchange and phosphate (oxygen)−water exchange reactions (MIX).[13,25,33−35] An isotopic upfield shift of the ^{31}P nuclear magnetic resonance upon binding of ^{18}O to phosphorus, of 3 Hz per ^{18}O, is observed, resulting in the appearance of new resonances.[25] Two MIX experiments were performed with MtGPP, the first starting with glycerol phosphate (Scheme 2A) and the second with P_i alone [without glycerol (Scheme 2B)].

MIX was first examined at 92% $H_2{}^{18}O$ for the hydrolysis of D,L-glycerol 3-phosphate (pH 7.5). Importantly, no exchange was observed in the absence of enzyme under identical conditions (results not shown). The spontaneous (enzyme-independent) ^{18}O isotope exchange between inorganic

dx.doi.org/10.1021/bi400856y | *Biochemistry* 2014, 53, 143−151

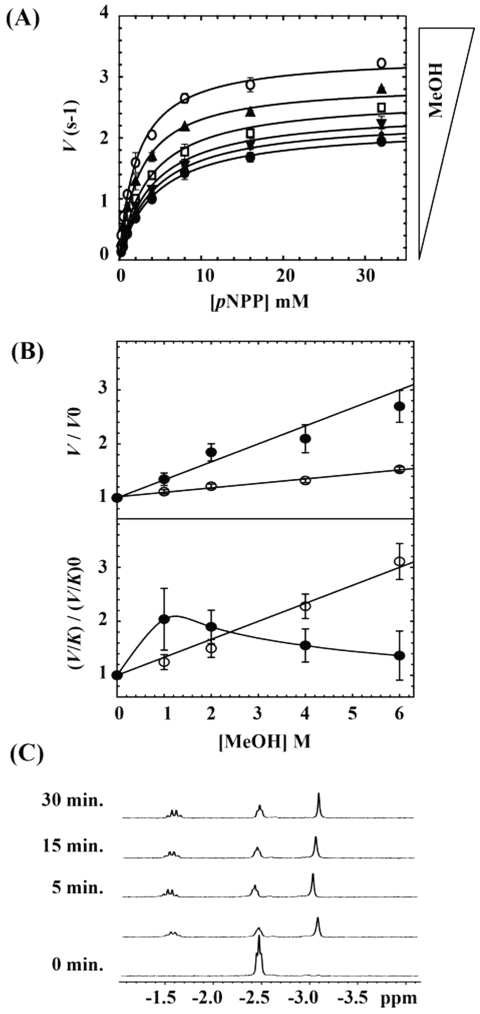

Figure 5. Partition experiments using methanol. (A) Saturation curves of *p*NPP with MtGPP at 0 (●), 0.5 (◆), 1 (▼), 2 (□), 4 (▲), and 6 M (○) MeOH, at pH 7.5. (B) Plot showing the ratio of rates obtained in the presence or absence of MeOH for V and V/K at pH 7.5 (○) and pH 6.0 (●). (C) Time course showing the formation of methylphosphate by one-dimensional $^{31}P-^{1}H$ coupled NMR.

Scheme 4. Proposed Chemical Mechanism of MtGPP

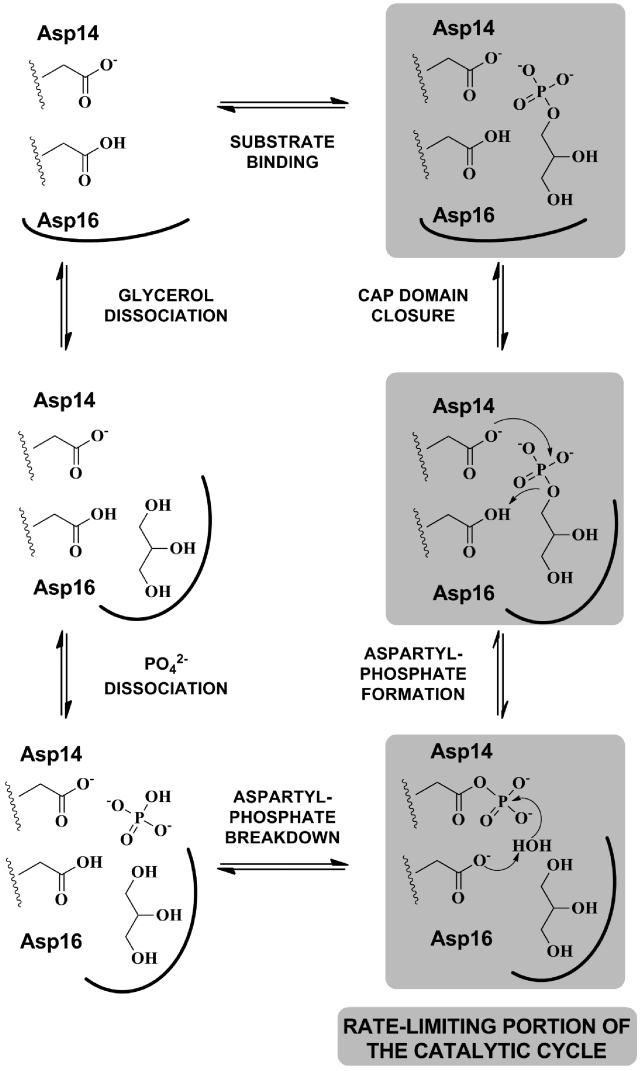

phosphate and water is negligible under the conditions tested (pseudo-first-order rate constant of 7.5×10^{-7} s^{-1} at 100 °C).[36] Figure 3A shows the time course of this reaction in the presence of MtGPP and demonstrates a distinct time-dependent incorporation of ^{18}O into P_i. The amount of each P_i species formed is summarized in Figure 3C. After 50 min, the reaction reached an apparent equilibrium, resulting in 31% [$P^{18}O^{16}O_3$], 61% [$P^{18}O_2{}^{16}O_2$], and 8% [$P^{18}O_3{}^{16}O_1$].

Next, Rv1962-catalyzed ^{18}O isotope exchange between P_i and water was investigated in the absence of glycerol (Figure 3B). No exchange was observed in the absence of MtGPP during the same period of incubation (results not shown). The shift in the signals observed for P_i in both experiments (Figure 3A,B) is due to the different amounts of EDTA in each sample. As for the hydrolysis of D,L-glycerol 3-phosphate, inorganic phosphate−water ^{18}O exchange is catalyzed by MtGPP, but in the latter case, the exchange is significantly slower: after incubation for 50 min, the resulting P_i pool is composed of 69% [$P^{16}O$], 26% [$P^{18}O^{16}O_3$], and 5% [$P^{18}O_2{}^{16}O_2$] (Figure 3D). Enzyme-catalyzed ^{18}O exchange between inorganic phosphate and water has been observed for a number of enzymes, including acid phosphatase,[23] alkaline phosphatase,[37,38] AT-Pases,[39] and low-molecular weight phosphotyrosyl protein phosphatase.[13] All these enzymes are known to proceed through a covalent phosphoenzyme intermediate. Therefore, our results indicate that MtGPP catalyzes ^{18}O exchange from D,L-glycerol 3-phosphate, as well as directly from P_i, via a phosphoenzyme intermediate. In addition, it is noteworthy that MIX was substantially accelerated in the presence of glycerol. This acceleration of the rate of exchange indicates that binding of P_i to MtGPP and formation of the aspartyl-phosphate intermediate are enhanced by glycerol, suggesting that P_i is the first product to dissociate, followed by glycerol.

Pre-Steady-State Kinetics Determined by Multiple-Turnover Experiments. To validate the occurrence of a rate-limiting conformational change during MtGPP catalysis (as inferred from SKIE and viscosity experiments), we conducted multiple-turnover experiments using *p*NPP as the substrate. These experiments were performed at pH 7.5, where chemistry was no longer rate-limiting at saturating concentrations of the substrate. If intermediate hydrolysis was rate-limiting, we would expect to see a burst of *p*-nitrophenolate production, indicating faster accumulation of preceding forms of the enzyme. However, if a slow step such as the postulated conformational

dx.doi.org/10.1021/bi400856y | *Biochemistry* 2014, 53, 143−151

change preceding chemistry is rate-limiting, no burst should be observed.

We performed pre-steady-state kinetic experiments under multiple-turnover conditions, at saturating concentrations of *p*NPP (40 mM) and various concentrations of MtGPP (5−100 μM). As one can see in Figure 4, time courses are linear for all concentrations of MtGPP used; no burst of product formation was observed. Moreover, a plot of k_{obs} versus the concentration of MtGPP was linear [slope of k = 0.751 ± 0.004 s^{-1} (inset, Figure 4)]. This rate is within experimental error of the k_{cat} for *p*NPP hydrolysis obtained under steady-state conditions (0.643 ± 0.085 s^{-1}). Altogether, these results support the existence of a rate-limiting conformational change preceding chemistry at pH ≥7.5.

Alternative Nucleophile Experiments. The SKIE results presented earlier indicate that chemistry is rate-limiting for MtGPP-catalyzed dephosphorylation at low pH and that conformational changes required for catalysis are rate-limiting at neutral and basic pH. To gain further insight into the chemical mechanism of the reaction, partition experiments were conducted in the presence of an alternative, stronger nucleophile, methanol (MeOH). Theory predicts that if the formation of the aspartyl-phosphate intermediate is the rate-limiting step, no increase in the reaction rate should be observed upon addition of MeOH. On the other hand, if breakdown of the aspartyl-phosphate intermediate is rate-limiting, addition of MeOH should accelerate the rate of the reaction. In both scenarios, the enzyme would be producing inorganic and methyl phosphate as final products (Scheme 3).

We determined steady-state kinetic parameters for MtGPP in the absence and presence of increasing concentrations of MeOH, at pH 6.0 (where chemistry is rate-limiting) and pH 7.5 (where chemistry is no longer rate-limiting) (Figure 5). Representative saturation curves obtained in the absence and presence of MeOH (0.5, 1, 2, 4, and 6 M) are shown in Figure 5A. We can observe an increase in V_{max} and K_m as the concentration of MeOH increases. These data can be represented as a ratio of their initial rate in the absence of MeOH (Figure 5B). We can observe that the rate of the reaction increases with increasing concentrations of MeOH, up to 6 M. At saturating concentrations of the substrate, V_{MeOH}/V_{H_2O} increased from 1.5 ± 0.1 at pH 7.5 to 2.7 ± 0.3 at pH 6.0 (Figure 5B, top panel). This result indicates that aspartyl-phosphate hydrolysis, probed under V conditions, is more rate-limiting at pH 6.0, in strict agreement with the results obtained from SKIE experiments. The dependence of V/K on methanol concentration was more complex (Figure 5B, bottom panel), and we did not attempt to interpret its significance. This increased complexity is probably due to a direct competition between methanol and glycerol binding sites, at low glycerol-phosphate concentrations.

An alternative interpretation of these results is that MeOH functions as an activator of MtGPP, perhaps through a conformational change, without directly acting as a nucleophile. To discriminate between these two sources of apparent activation kinetics, we investigated the production of methyl phosphate, by one-dimensional $^{31}P-^{1}H$ coupled NMR. Figure 5C illustrates the time course of catalytic conversion of D,L-glycerol 3-phosphate (triplet at approximately −2.5 ppm) in the presence of 6 M MeOH. Under these conditions, the ^{31}P peak attributed to D,L-glycerol 3-phosphate should be a triplet, the P_i peak should be a singlet, and the peak for methylphosphate should be a quartet because of the presence of two, zero, and three carbon-bound protons vicinal to the phosphorus nuclei, respectively. Time-dependent formation of phosphate (singlet at approximately −3.1 ppm) and methyl phosphate (quartet at −1.5 ppm) is clearly observed, directly implicating MeOH as a substrate for the breakdown of the aspartyl-phosphate intermediate.

Altogether, the methanolysis results obtained confirm that the breakdown of the aspartyl-phosphate intermediate is partially rate-limiting at pH 6.0.

Proposed Mechanism. The proposed mechanism, depicted in Scheme 4, starts with binding of glycerol 3-phosphate to MtGPP. This binding step is likely followed by a conformational change, prior to catalysis. The conserved Asp14 (pK_a ∼ 6.0) attacks glycerol 3-phosphate, breaking the P−O−C bond forming the aspartyl-phosphate intermediate and glycerolate, which abstracts a proton from Asp16. This overall step is partially rate-limiting below pL 7.0. Asp16 activates a water molecule that attacks the aspartyl-phosphate intermediate, generating inorganic phosphate. This step is also partially rate-limiting below pL 7.0. Inorganic phosphate dissociates from MtGPP followed by glycerol, generating free enzyme.

■ ASSOCIATED CONTENT

Supporting Information

pH dependence of the extinction coefficient of *p*-nitrophenolate (Table S1), dependence of V/K and V on pH at saturating concentrations of *p*NPP (Figure S1), dependence of V/K and V on pL (Figure S2), pH dependence of $^{D_2O}V/K$ (Figure S3), pH dependence of ^{D_2O}V (Figure S4), and effect of NaCl on the kinetic parameters of MtGPP-catalyzed hydrolysis of pNPP (Figure S5). This material is available free of charge via the Internet at http://pubs.acs.org.

■ AUTHOR INFORMATION

Corresponding Author

*MRC National Institute for Medical Research, The Ridgeway, Mill Hill, London NW7 1AA, United Kingdom. E-mail: luiz.pedro@nimr.mrc.ac.uk. Telephone: +44 (0)20 8816 2358. Fax: +44 (0)20 8816 2358.

Author Contributions

G.L.-M. and G.K. performed experiments. G.L.-M. and L.P.S.d.C. designed, analyzed, and interpreted experiments. G.L.-M. and L.P.S.d.C. wrote the manuscript.

Funding

This work was supported by funds from the MRC to L.P.S.d.C. (MC_UP_A253_1111). The MRC Biomedical NMR Centre, NIMR, Mill Hill, is funded by MRC Grant-in-Aid U117533887.

Notes

The authors declare no competing financial interest.

■ ACKNOWLEDGMENTS

We thank Dr. Steve Howell for ESI-MS analysis of purified MtGPP, the NIMR's Large Scale Laboratory for *E. coli* growth, and Dr. Gareth A. Prosser for critical reading of the manuscript.

■ ABBREVIATIONS

Asp, aspartic acid; BCA, bicinchoninic acid assay; GNAT, GCN5-related *N*-acetyltransferase; HADSF, halo-acid dehalogenase superfamily; MeOH, methanol; MIX, molecular isotope

exchange; Mtb, *M. tuberculosis*; SKIE, solvent kinetic isotope effect.

REFERENCES

(1) Lahiri, S. D., Zhang, G., Dunaway-Mariano, D., and Allen, K. N. (2002) Caught in the act: The structure of phosphorylated β-phosphoglucomutase from *Lactococcus lactis*. *Biochemistry 41*, 8351−8359.

(2) Toyoshima, C., Nakasako, M., Nomura, H., and Ogawa, H. (2000) Crystal structure of the calcium pump of sarcoplasmic reticulum at 2.6 Å resolution. *Nature 405*, 647−655.

(3) Diaz, A. R., Stephenson, S., Green, J. M., Levdikov, V. M., Wilkinson, A. J., and Perego, M. (2008) Functional role for a conserved aspartate in the Spo0E signature motif involved in the dephosphorylation of the *Bacillus subtilis* sporulation regulator Spo0A. *J. Biol. Chem. 283*, 2962−2972.

(4) Kim, Y., Gentry, M. S., Harris, T. E., Wiley, S. E., Lawrence, J. C., Jr., and Dixon, J. E. (2007) A conserved phosphatase cascade that regulates nuclear membrane biogenesis. *Proc. Natl. Acad. Sci. U.S.A. 104*, 6596−6601.

(5) Ghosh, A., Shuman, S., and Lima, C. D. (2008) The structure of Fcp1, an essential RNA polymerase II CTD phosphatase. *Mol. Cell 32*, 478−490.

(6) Deshpande, R. A., and Wilson, T. E. (2004) Identification of DNA 3′-phosphatase active site residues and their differential role in DNA binding, Mg^{2+} coordination, and catalysis. *Biochemistry 43*, 8579−8589.

(7) Cho, H., Wang, W., Kim, R., Yokota, H., Damo, S., Kim, S. H., Wemmer, D., Kustu, S., and Yan, D. (2001) BeF_3^- acts as a phosphate analog in proteins phosphorylated on aspartate: Structure of a BeF_3^- complex with phosphoserine phosphatase. *Proc. Natl. Acad. Sci. U.S.A. 98*, 8525−8530.

(8) Lahiri, S. D., Zhang, G., Dai, J., Dunaway-Mariano, D., and Allen, K. N. (2004) Analysis of the substrate specificity loop of the HAD superfamily cap domain. *Biochemistry 43*, 2812−2820.

(9) Allen, K. N., and Dunaway-Mariano, D. (2004) Phosphoryl group transfer: Evolution of a catalytic scaffold. *Trends Biochem. Sci. 29*, 495−503.

(10) Burroughs, A. M., Allen, K. N., Dunaway-Mariano, D., and Aravind, L. (2006) Evolutionary genomics of the HAD superfamily: Understanding the structural adaptations and catalytic diversity in a superfamily of phosphoesterases and allied enzymes. *J. Mol. Biol. 361*, 1003−1034.

(11) Lu, Z., Wang, L., Dunaway-Mariano, D., and Allen, K. N. (2009) Structure-function analysis of 2-keto-3-deoxy-D-glycero-D-galactonononate-9-phosphate phosphatase defines specificity elements in type C0 haloalkanoate dehalogenase family members. *J. Biol. Chem. 284*, 1224−1233.

(12) Zhang, Z. Y. (1995) Kinetic and mechanistic characterization of a mammalian protein-tyrosine phosphatase, PTP1. *J. Biol. Chem. 270*, 11199−11204.

(13) Zhang, Z. Y., and VanEtten, R. L. (1991) Pre-steady-state and steady-state kinetic analysis of the low molecular weight phosphotyrosyl protein phosphatase from bovine heart. *J. Biol. Chem. 266*, 1516−1525.

(14) McCain, D. F., Grzyska, P. K., Wu, L., Hengge, A. C., and Zhang, Z. Y. (2004) Mechanistic studies of protein tyrosine phosphatases YopH and Cdc25A with m-nitrobenzyl phosphate. *Biochemistry 43*, 8256−8264.

(15) Picha, K. M., Patel, S. S., Mandiyan, S., Koehn, J., and Wennogle, L. P. (2007) The role of the C-terminal domain of protein tyrosine phosphatase-1B in phosphatase activity and substrate binding. *J. Biol. Chem. 282*, 2911−2917.

(16) Zhang, Z. Y., and Van Etten, R. L. (1991) Leaving group dependence and proton inventory studies of the phosphorylation of a cytoplasmic phosphotyrosyl protein phosphatase from bovine heart. *Biochemistry 30*, 8954−8959.

(17) Hengge, A. C., Zhao, Y., Wu, L., and Zhang, Z. Y. (1997) Examination of the transition state of the low-molecular mass small tyrosine phosphatase 1. Comparisons with other protein phosphatases. *Biochemistry 36*, 7928−7936.

(18) Hiwada, K., and Wachsmuth, E. D. (1974) Catalytic properties of alkaline phosphatase from pig kidney. *Biochem. J. 141*, 283−291.

(19) Catrina, I., O'Brien, P. J., Purcell, J., Nikolic-Hughes, I., Zalatan, J. G., Hengge, A. C., and Herschlag, D. (2007) Probing the origin of the compromised catalysis of *E. coli* alkaline phosphatase in its promiscuous sulfatase reaction. *J. Am. Chem. Soc. 129*, 5760−5765.

(20) Huang, T. M., Hung, H. C., Chang, T. C., and Chang, G. G. (1998) Solvent kinetic isotope effects of human placental alkaline phosphatase in reverse micelles. *Biochem. J. 330* (Part 1), 267−275.

(21) Anderson, R. A., Bosron, W. F., Kennedy, F. S., and Vallee, B. L. (1975) Role of magnesium in *Escherichia coli* alkaline phosphatase. *Proc. Natl. Acad. Sci. U.S.A. 72*, 2989−2993.

(22) Anderson, R. A., Kennedy, F. S., and Vallee, B. L. (1976) The effect of Mg(II) on the spectral properties of Co(II) alkaline phosphatase. *Biochemistry 15*, 3710−3716.

(23) Van Etten, R. L., and Risley, J. M. (1978) Phosphate (oxygen)-water exchange reaction catalyzed by human prostatic acid phosphatase. *Proc. Natl. Acad. Sci. U.S.A. 75*, 4784−4787.

(24) Larrouy-Maumus, G., Biswas, T., Hunt, D. M., Kelly, G., Tsodikov, O. V., and de Carvalho, L. P. (2013) Discovery of a glycerol 3-phosphate phosphatase reveals glycerophospholipid polar head recycling in *Mycobacterium tuberculosis*. *Proc. Natl. Acad. Sci. U.S.A. 110*, 11320−11325.

(25) Cohn, M., and Hu, A. (1978) Isotopic (^{18}O) shift in ^{31}P nuclear magnetic resonance applied to a study of enzyme-catalyzed phosphate−phosphate exchange and phosphate (oxygen)−water exchange reactions. *Proc. Natl. Acad. Sci. U.S.A. 75*, 200−203.

(26) Cleland, W. W. (1977) Determining the chemical mechanisms of enzyme-catalyzed reactions by kinetic studies. *Adv. Enzymol. Relat. Areas Mol. Biol. 45*, 273−387.

(27) Cleland, W. W. (1982) The use of pH studies to determine chemical mechanisms of enzyme-catalyzed reactions. *Methods Enzymol. 87*, 390−405.

(28) Cook, P. F., and Clelland, W. W. (2007) *Enzyme Kinetics and Mechanism*, Taylor & Francis, LLC, New York.

(29) Karsten, W. E., Lai, C. J., and Cook, P. F. (1995) Inverse Solvent Isotope Effect in NAD-Malic Enzyme Reaction Are the Result of the Viscosity Difference between D_2O and H_2O: Implications for Solvent Isotope Effect Studies. *J. Am. Chem. Soc. 117*, 5914−5918.

(30) Quinn, D. M., and Sutton, L. D. (1991) *Theoretical Basis and Mechanistic Utility of Solvent Isotope Effects* (Cook, P. F., Ed.) CRC Press, Boca Raton, FL.

(31) Raber, M. L., Freeman, M. F., and Townsend, C. A. (2009) Dissection of the stepwise mechanism to β-lactam formation and elucidation of a rate-determining conformational change in β-lactam synthetase. *J. Biol. Chem. 284*, 207−217.

(32) Lahiri, S. D., Zhang, G., Dunaway-Mariano, D., and Allen, K. N. (2003) The pentacovalent phosphorus intermediate of a phosphoryl transfer reaction. *Science 299*, 2067−2071.

(33) Raushel, F. M., and Villafranca, J. J. (1980) Phosphorus-31 nuclear magnetic resonance application to positional isotope exchange reactions catalyzed by *Escherichia coli* carbamoyl-phosphate synthetase: Analysis of forward and reverse enzymatic reactions. *Biochemistry 19*, 3170−3174.

(34) Zhang, Z. Y., Zhou, G., Denu, J. M., Wu, L., Tang, X., Mondesert, O., Russell, P., Butch, E., and Guan, K. L. (1995) Purification and characterization of the low molecular weight protein tyrosine phosphatase, Stp1, from the fission yeast *Schizosaccharomyces pombe*. *Biochemistry 34*, 10560−10568.

(35) Kounga, K., Vander Velde, D. G., and Himes, R. H. (1995) ^{18}Oxygen incorporation into inorganic phosphate in the reaction catalyzed by N5,10-methenyltetrahydrofolate synthetase. *FEBS Lett. 364*, 215−217.

(36) Hackney, D. D., and Boyer, P. D. (1978) Evaluation of the partitioning of bound inorganic phosphate during medium and intermediate phosphate in equilibrium water oxygen exchange

reactions of yeast inorganic pyrophosphatase. *Proc. Natl. Acad. Sci. U.S.A. 75*, 3133−3137.
(37) Eargle, D. H., Jr., Licko, V., and Kenyon, G. L. (1977) Kinetic studies of ^{18}O exchange of inorganic phosphate using mass spectral measurements on the tris-(trimethylsilyl) derivative. *Anal. Biochem. 81*, 186−195.
(38) Applebury, M. L., Johnson, B. P., and Coleman, J. E. (1970) Phosphate binding to alkaline phosphatase. Metal ion dependence. *J. Biol. Chem. 245*, 4968−4976.
(39) Faller, L. D., and Diaz, R. A. (1989) Evidence from ^{18}O exchange measurements for steps involving a weak acid and a slow chemical transformation in the mechanism of phosphorylation of the gastric H^+,K^+-ATPase by inorganic phosphate. *Biochemistry 28*, 6908−6914.